Chinese Chemical Letters 35 (2024) 109554

Contents lists available at ScienceDirect

Chinese Chemical Letters

journal homepage: www.elsevier.com/locate/cclet

Multifunctional 2-(2′-hydroxyphenyl)benzoxazoles: Ready synthesis, mechanochromism, fluorescence imaging, and OLEDs

Kangmin Wang[a], Liqiu Wan[a], Jingyu Wang[c], Chunlin Zhou[a], Ke Yang[b,*], Liang Zhou[c,*], Bijin Li[a,b,*]

[a] Chongqing Key Laboratory of Natural Product Synthesis and Drug Research, School of Pharmaceutical Sciences, Chongqing University, Chongqing 401331, China
[b] Jiangsu Key Laboratory of Advanced Catalytic Materials & Technology, School of Petrochemical Engineering, Changzhou University, Changzhou 213164, China
[c] State Key Laboratory of Rare Earth Resource Utilization, Changchun Institute of Applied Chemistry, Chinese Academy of Sciences, Changchun 130022, China

ARTICLE INFO

Article history:
Received 5 October 2023
Revised 10 January 2024
Accepted 19 January 2024
Available online 23 January 2024

Keywords:
Rhodium-catalyzed
2-(2′-Hydroxyphenyl)benzoxazoles
Mechanochromism
Fluorescence images
OLEDs

ABSTRACT

Triphenylamine (TPA)-containing 2-(2′-hydroxyphenyl)benzoxazoles (**2a-2c**) have been synthesized *via* a highly efficient rhodium-catalyzed C–H/C–H cross-coupling reaction. Compound **2a** is a novel mechanofluorochromic material with blue-shifted mechanochromic properties. Compounds **2b** and **2c** presented opposite mechanochromic trends. For **2b**, the enol-form emission enhanced, and the keto-form emission blue-shift after grinding. In contrast, **2c** exhibited the weak enol-form emission disappeared and the keto-form emission slightly red-shift after grinding treatments. The estrone-containing **2b**-based water-dispersed nanoparticles (NPs) exhibit apparent dual-emission and were applied for fluorescence images. In addition, bis(TPA)-containing **2c**-based devices exhibit dual-emission with good performance and a singlet exciton yield of 92%, which breaks through the theoretical upper limit of 25% in conventional fluorescent OLEDs. This is one of the highest exciton utilization values recorded for the ESIPT molecules with a dual emission system.

High-performance organic fluorescent materials are of great interest to chemical and medical scientists because they can be applied in mechanochromic devices, security systems, fluorescence imaging, organic light-emitting diodes (OLEDs), *etc.* [1–24]. At present, the reported excited state intramolecular proton transfer (ESIPT) fluorescent materials based on 2-(2′-hydroxyphenyl)benzoxazoles feature planarity due to the intramolecular hydrogen-bonding fixation on the dihedral angle of the diaryl skeleton and, therefore, are apt to aggregate in the solid state, resulting in a quenching enol-form or weak keto-form emission, which is unfavorable for mechanochromic luminescence applications, imaging, and high-performance OLEDs fabrication [4–7,25-28]. Therefore, developing high-performance ESIPT fluorescent materials based on 2-(2′-hydroxyphenyl)benzoxazoles is still highly desirable.

Herein, we constructed high-performance fluorescent materials based on triphenylamine (TPA)-containing 2-(2′-hydroxyphenyl) benzoxazoles (**2a-2c**) using the efficient Rh(III)-catalyzed oxidative C–H/C–H cross-coupling reaction (Scheme 1). The phenol-containing natural product estrone underwent the coupling with **S1** to afford product **2b** with a 67% yield. Furthermore, 2-(benzo[*d*]oxazol-2-yl)phenol (**2aa**) has also been synthesized as a reference molecule (Fig. 1, Section III in Supporting information). The emission spectra of compounds **2a-2c** and **2aa** were measured in toluene and shown in Fig. 1. Compound **2aa** without a strongly electron-donating TPA group only displays the excited-state intramolecular proton transfer (ESIPT) keto-form emission at 487 nm with a low fluorescence quantum yield (2.0%) in toluene. TPA-containing **2a** exhibits sole the enol-form emission at 417 nm with a higher fluorescence quantum yield (25.6%) than **2aa** in toluene.

Compound **2aa** is a classical ESIPT molecule, and its mechanism has been confirmed (Fig. 1 and Fig. S1a in Supporting information) [3–7]. For TPA-containing 2-(2′-hydroxyphenyl)benzoxazoles (**2a**), the energy level of the keto-form is higher than that of the enol form in the lowest excited (Fig. 1 and Fig. S1b in Supporting information). As a result, **2a** only exhibits sole the enol-form emissions and lack of keto-form emission (Fig. 1d). Moreover, **2a** also displays sole the enol-form emission in other solutions (Fig. S3 in Supporting information). Bis(TPA)-containing **2c** shows the weak enol-form emission and the strong keto-form emission in toluene

* Corresponding authors.
E-mail addresses: keyang@cczu.edu.cn (K. Yang), zhoul@ciac.ac.cn (L. Zhou), bijinli@cqu.edu.cn (B. Li).

https://doi.org/10.1016/j.cclet.2024.109554
1001-8417/

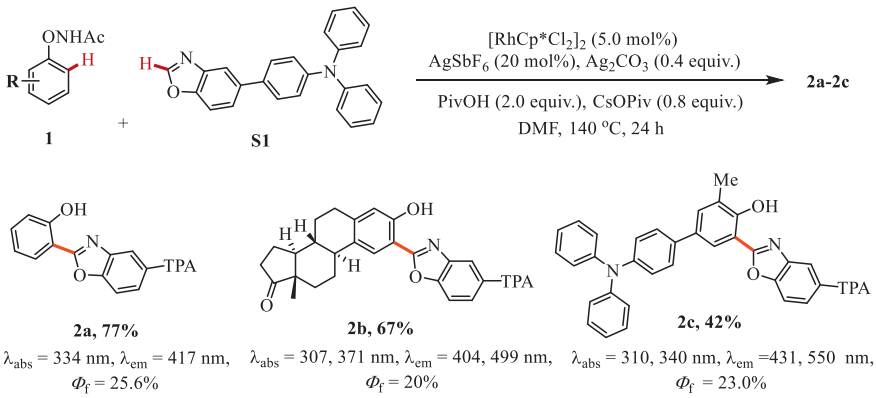

Scheme 1. Synthesis of TPA-containing 2-(2′-hydroxyphenyl)benzoxazoles (**2a-2c**) and their photophysical properties in toluene solution (5×10^{-5} mol/L). Absolute quantum yield was determined with a calibrated integrating sphere system.

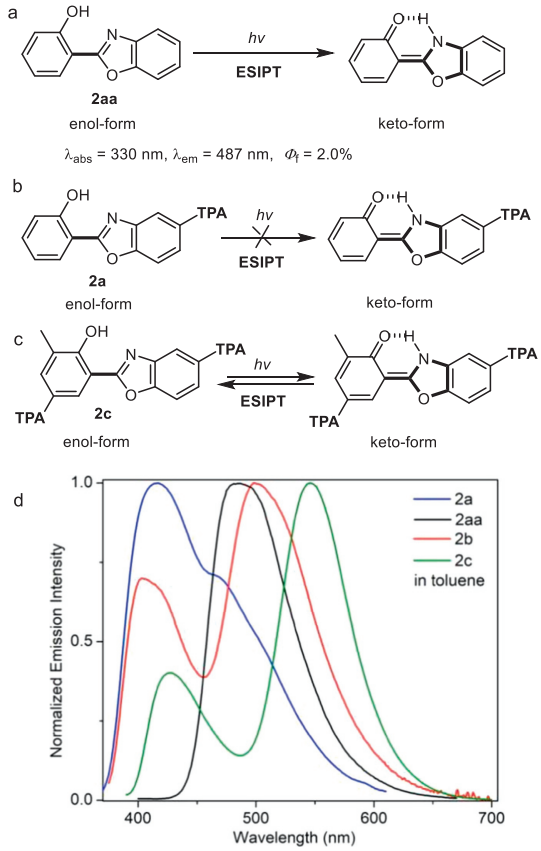

Fig. 1. (a) ESIPT mechanism of **2aa**; photophysical properties in toluene solution (5×10^{-5} mol/L). (b) ESIPT mechanism of **2a**. (c) ESIPT mechanism of **2c**. (d) Emission spectra of **2a-2c** in toluene solution (5×10^{-5} mol/L).

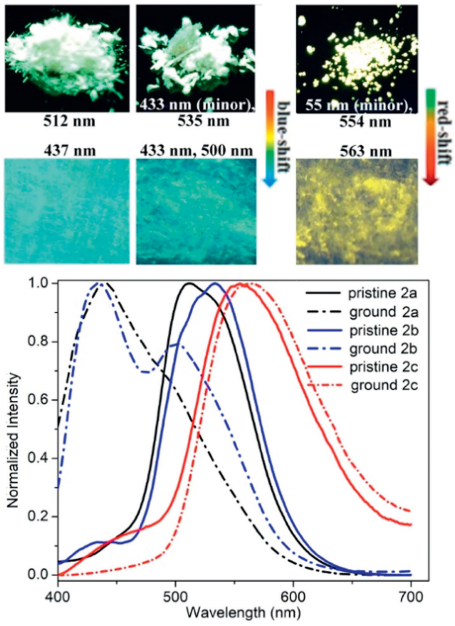

Fig. 2. The fluorescent images (under UV light) and emission spectra of **2a-2c** before and after grinding ($\lambda_{ex} = 370$ nm).

(Fig. 1 and Fig. S1c in Supporting information). The excited-state enol form of the **2c** has a close energy level with its keto form. In addition, the fluorescence quantum yields of **2b-2c** were measured to be 20% and 23% respectively. These results demonstrate that TPA-containing 2-(2′-hydroxyphenyl)benzoxazoles are a novel fluorescent material.

Subsequently, the mechanochromic luminescence properties of **2a-2c** were investigated. Grinding of pristine powder **2a** displays a blue shift with an emission color change from yellow-green ($\lambda_{em} = 512$ nm) to blue ($\lambda_{em} = 437$ nm), approximately 75 nm (Fig. 2). The reference compound **2aa** does not exhibit piezochromic behavior. For **2b**, a significant enhancement of the enol-form emission at 433 nm is observed after grinding, and its keto-form emission is blue-shifted from 535 nm to 500 nm (Fig. 2). The ratio of the two emission peaks remarkably changes before and after grinding. After grinding, the intensity of the enol-form emission of **2b** exceeds its keto-form emission. The weak enol-form emission of bis(TPA)-containing **2c** almost disappears and the strong keto-form emission induces a slight red-shift after grinding treatment (Fig. 2).

To gain insight into the piezochromic mechanism, the phase characteristics of **2a** were studied by differential scanning calorimetry (DSC) and powder X-ray diffraction (PXRD) analysis. A transition between the metastable state and the stable state of **2a** was found because the ground of **2a** presented a slight exothermal peak in the DSC experiment (Fig. S6 in Supporting information). In addition, the crystalline morphological transition to amorphous phases was demonstrated due to the pristine **2a** showing sharp and intense reflection peaks and corresponding sharp peaks disappearing at the ground **2a** state (Fig. S7 in Supporting information). We further obtained two single crystals of yellowish-green-emitting **2bs$_1$** (CCDC: 2261804) and green-emitting **2bs$_2$** (CCDC: 2261803) by slow diffusion of EtOH or n-hexane vapor into a solu-

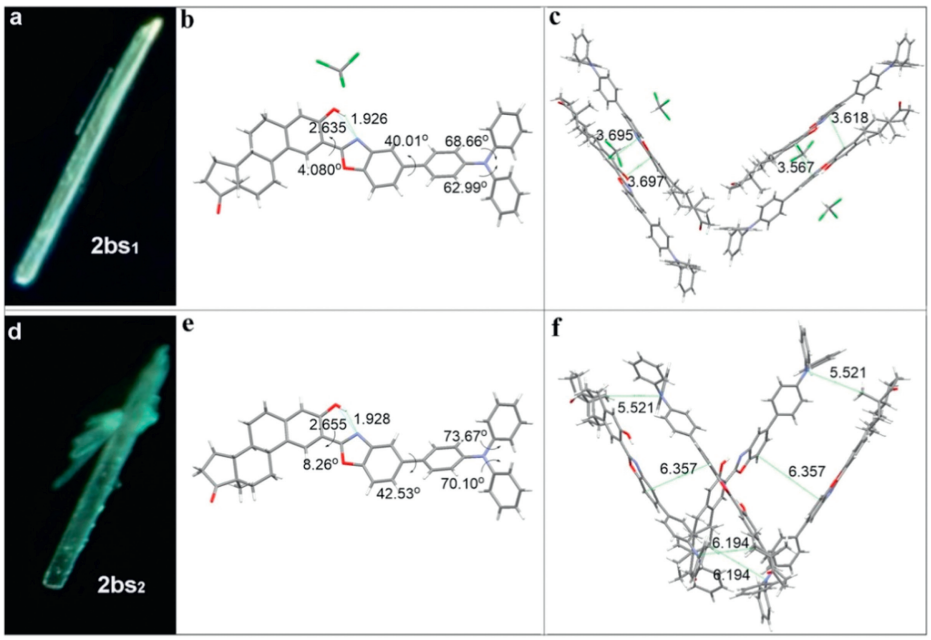

Fig. 3. (a) Photograph of single crystal of $\mathbf{2bs_1}$ under UV light (365 nm). (b) The yellowish-green-emitting single crystal $\mathbf{2bs_1}$ (CCDC: 2261804) and (c) its packing motif. (d) Photograph of single crystal of $\mathbf{2bs_2}$ under UV light (365 nm). (e) The green-emitting single crystal $\mathbf{2bs_2}$ (CCDC: 2261803) and (f) its packing motif.

tion of **2b** in $CHCl_3$ at room temperature (Fig. 3 and Fig. S8 in Supporting information). The yellowish-green-emitting single crystal $\mathbf{2bs_1}$ shows emission peaks at 433 nm (minor) and 518 nm, which is close to those of pristine **2b**. Furthermore, by grinding the crystal, the enol-form emission is enhanced, and keto-form emission is slightly blue-shifted, which shows the apparent dual-emission of the enol-form ($\lambda_{em} = 433$ nm) and keto-form ($\lambda_{em} = 503$ nm) (Fig. S9 in Supporting information). The single crystal $\mathbf{2bs_1}$ exhibits a twisted conformation and a strong π–π stacking mode. Although the benzoxazole group and phenol are close to coplanar and have a dihedral angle of 4.08°, the dihedral angle between the benzoxazole ring and the phenyl plane in the TPA is 40.01°.

Moreover, the dihedral angles between the phenyl and the other two phenyls in the TPA reveal 62.99° and 68.66° (Fig. 3). The green-emitting single crystal $\mathbf{2bs_2}$ exhibits a weak enol-form emission ($\lambda_{em} = 433$ nm) and a strong keto-form emission ($\lambda_{em} = 503$ nm) (Fig. S9). By grinding the crystal $\mathbf{2bs_2}$, the two emission peak positions almost keep unchanged. However, the enol-form emission significantly enhanced, which roughly coincides with those of ground **2b** (Fig. S9). The single crystal $\mathbf{2bs_2}$ reveals 70.10°–73.67° dihedral angles between the phenyl and the other two phenyls in the TPA, and a 42.53° dihedral angle between the benzoxazole ring and the phenyl plane in the TPA. Two molecules are stacked in reverse parallel with distances of 3.567–3.697 Å, and four molecules form a V-shaped structure in the single crystal $\mathbf{2bs_1}$ (Fig. 3). The shorter distance and tight molecular packing indicate potential π–π stacking among neighboring molecules. The single crystal of $\mathbf{2bs_2}$ shows the reverse parallelism of two molecules with distances of 5.521–6.357 Å. These results demonstrate that the green-emitting single crystal $\mathbf{2bs_2}$ displays a more distorted conformation and loose accumulation than the yellowish-green-emitting single crystal of $\mathbf{2bs_1}$.

Thus, the emission of **2a** and keto-form emission of **2b** are blue-shifted after grinding their powders can be ascribed to lessened coplanarity of molecules and weakened intermolecular π–π interactions. The enhanced enol-form emission of **2b**, and the disappeared enol-form emission of **2c** after grinding may be attributed to a new ESIPT equilibrium accompanied by changes in the molecular packing modes, molecular planarity, and intramolecular hydrogen-bond strength [15]. Furthermore, the external force stimuli can strengthen intermolecular π–π stacking interactions, which leads to a slight red-shifted keto-emission of **2c**. In addition, a shift of the ESIPT equilibrium towards an enhanced keto-form emission in the solid leads to **2c** showing the very weak enol-form emission and the strong keto-form emission. After grinding, the disappearance of very weak enol-form emission, and a slight red-shifted keto-emission result in the **2c** displays inconspicuous mechanofluorochromism (Fig. 2).

Furthermore, using Poloxamer 188 as a matrix, the estrone-containing **2b** was fabricated as water-dispersed nanoparticles (NPs) through a thin-film hydration method (Fig. S10 in Supporting information). The **2b** NPs exhibit an apparent dual-emission of the enol-form ($\lambda_{em} = 441$ nm) and keto-form ($\lambda_{em} = 503$ nm) (Fig. 4a). Dynamic light scattering (DLS) measurement indicates that **2b** NPs have a hydrodynamic diameter of about 76.4 nm (polydispersity index value of 0.136) (Fig. 4b). Scanning electron microscopy (SEM) images reveal that the **2b** NPs have a well-defined spherical shape with diameters of approximately about 80 nm (Fig. S13 in Supporting information), which are roughly equal in size to those of DLS measurement. Such appropriate nanoscale sizes have great potential for fluorescence imaging of tumor cells *via* enhanced permeability and retention effects [20]. Besides, the zeta potential of the as-prepared **2b** NPs is approximately 18.38 mV.

To assess the safe usability of **2b** NPs for biomedical applications, the cytotoxicity experiments in HeLa cells were conducted using the standard methyl thiazolyl tetrazolium (MTT) assay (Fig. S14 in Supporting information). The cell viability values demonstrated that **2b** NPs show almost no toxicity in HeLa cells (Fig. S14). Even at a high concentration, **2b** NPs do not exhibit significant cytotoxicity, further confirming its good biocompatibility. To gain study the cellular imaging capability of **2b** NPs, staining experiments of **2b** NPs in HeLa cells were performed, and then the fluorescent images were captured by confocal laser scanning microscopy (CLSM). The single-photon-excited blue-green fluorescence signal can be observed in HeLa cells after being treated with the **2b** NPs for 2 h (Figs. 4c and d, Figs. S15 and S16 in Supporting information). In addition, the cellular two-photon-excited imaging capability of **2b** NPs was employed in HeLa cells using CLSM

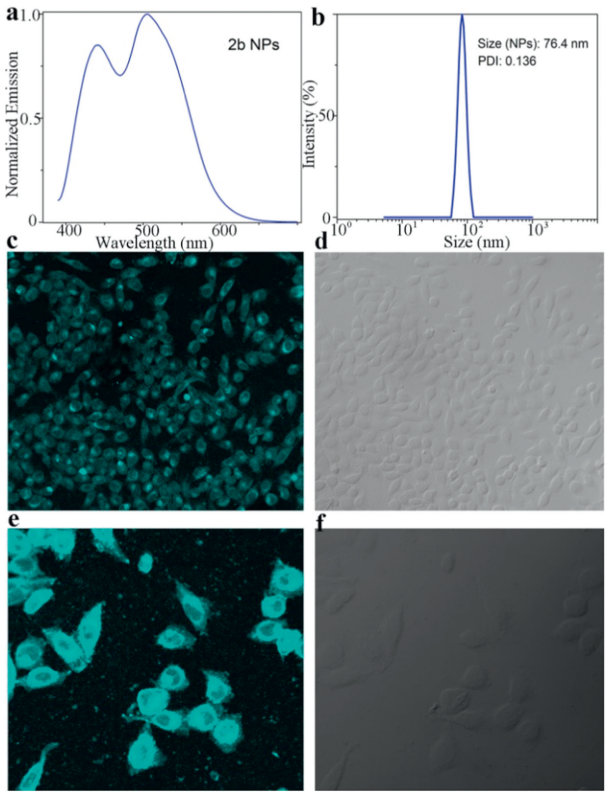

Fig. 4. (a) The fluorescence spectrum of the **2b** NPs. (b) Size distribution of the **2b** NPs. (c) The single-photon-excited confocal laser scanning microscopy fluorescence imaging **2b** nanoparticles channel, (d) bright field. (e) Two-photon-excited confocal laser scanning microscopy fluorescence imaging **2b** nanoparticles channel, (f) bright field.

equipped with a femtoseconds laser. The obvious blue-green fluorescence signals were detected in HeLa cells by two-photon irradiation, indicating that **2b** NPs have admirable two-photon excitation fluorescence imaging properties (Figs. 4e and f, Figs. S15 and S16). Thus, we conclude that the **2b** NPs can be efficiently endocytosed into the HeLa cells and applied for blue-green imaging probes, which is the first reported of dual emission ESIPT systems with promising potential in both single-photon-excited and two-photon-excited fluorescence imaging [3–7].

Organic fluorescent molecules with the hybridized local charge transfer (HLCT)-state character were considered high-performance fluorescent materials that can favor improving the utilization of OLED excitons [29–34]. Our recent research has shown that the electron-donating TPA group can adjust the energetics of ESIPT and endow molecules to have the hybridized local charge transfer (HLCT)-state feature [35]. In addition, the thermal and electrochemical properties of **2c** were studied (Table S1, Figs. S17 and S18 in Supporting information), indicating that it was suitable for vacuum thermal sublimation for OLED fabrication. Hence, the electroluminescence properties of bis(TPA)-containing **2c** in OLED devices were further surveyed.

The devices A-F were fabricated with the structure of ITO/MoO_3 (3 nm)/TAPC (50 nm)/**2c** (x wt%): CBZ_2-F_1 or TBCPF (20 nm)/$Tm_3PyP_{26}PyB$ (50 nm)/LiF (1 nm)/Al (100 nm) (Part X in Supporting information). The molecular structures and energy levels of the devices were shown in Fig. S19 (Supporting information). Device D based on **2c** (6 wt%) in CBZ_2-F_1 shows a low turn-on voltage and good performance with the maximum EQE (EQE_{max}), brightness (L_{max}), power efficiency (PE_{max}), current efficiency (CE_{max}), and CIE coordinates of 3.4 V, 3.5%, 8338 cd/m^2, 11.5 cd/A, 10.7 lm/W and (0.30, 0.52), respectively (Table S2 and Fig.

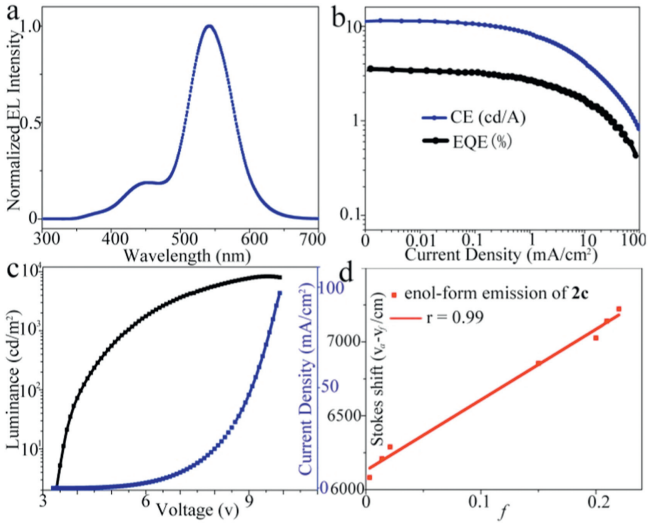

Fig. 5. (a) Normalized EL spectra of device at 3.4 V. (b) The EL efficiency–current density curve and EQE–current density curve of device. (c) Luminance–current density–voltage (L–J–V) characteristics of the device. (d) Linear fitting of Lippert–Mataga model (enol-form emission of **2c**).

5). The exciton utilization (η_S) of device D was calculated by equation below:

$$\eta_s = EQE_{max}/(\eta_{out} \times \eta_{PL} \times \gamma)$$
$$= 3.5\%/(100\% \times 19\% \times 20\%)$$
$$= 92\%$$

where η_{out}, η_{PL}, γ is the light-out-coupling efficiency, the photoluminescence (PL) efficiency of **2c** (6 wt% in CBZ_2-F_1), and the recombination probability of hole–electron in the emission layer, respectively. The exciton utilization of device D breaks through the theoretical limit of 25% in conventional fluorescent OLEDs. The singlet exciton yield of up to 92% is the one of highest exciton utilization value recorded for the ESIPT molecules with a dual emission system [35–39].

The HLCT state character of **2c** was further studied by the solvation effects on absorption and emission in different solvents (Fig. S21 and Section XI in Supporting ingormation). The vibrational fine structure is found from the PL spectrum of **2c** in *n*-hexane, which demonstrates the existence of the LE state [35,37,40]. The enol-form emission of **2c** exhibits a gradually red-shifted solvatochromic behavior, whereas its keto-form emissions have only a slight change in the solvent polarity [35,37,40]. Its enol form exhibits only one slope value of 4781 ($r = 0.99$) in the linear fitting of the Lippert–Mataga model (Fig. 5d and Fig. S21), demonstrating the CT feature of **2c** in the excited state. The excited state dipole moment (μ_e) was estimated to be 15.8 D, which is larger than that of usual LE emitters (*ca.* 8 D) and smaller than that of the typical CT molecule 4-(*N*,*N*-dimethylamino)benzonitrile (*ca.* 23 D) [35,37,40-43]. Furthermore, the HOMO and LUMO of **2c** have intercrossed molecular orbitals, leading to an intercrossed transition of CT and $\pi \rightarrow \pi^*$ and bringing the intercrossed character of the LE and CT states (Fig. S23 in Supporting information) [35,43]. Moreover, the PL lifetimes of **2c** in solvent and film were investigated (Fig. S22 and Table S4 in Supporting information). Only several lifetime components with nanosecond order were detected, and delayed fluorescence components have not found [35,43].

In summary, the high-performance and multifunctional fluorescent materials based on TPA-containing 2-(2′-hydroxyphenyl) benzoxazoles (**2a-2c**) were obtained efficiently by rhodium-catalyzed C–H activation reaction. Compound **2a** exhibit sole the enol-form emission with a high fluorescence quantum yield

and blue-shifted piezochromic luminescence properties. The ESIPT molecule **2b** displays significantly enhanced enol-form emission, as well as blue-shifted keto-form emission after grinding. In contrast, bis(TPA)-containing **2c** shows the weak enol-form emission disappeared and the strong keto-form emission slightly red-shift after grinding treatments. This discovery represents the first example of opposite mechanochromic trends in ESIPT molecules with a dual emission system. The piezochromic blue shift after grinding can be ascribed to lessened coplanarity of molecules and weakened intermolecular $\pi-\pi$ interactions, and the enol-form emission alteration after grinding may be attributed to a new ESIPT equilibrium accompanied by changes in the molecular packing modes, molecular planarity, and intramolecular hydrogen-bond strength. The estrone-containing **2b** has been fabricated as water-dispersed NPs and exhibited an apparent dual-emission. The NPs further were used as a blue-green imaging probe in both single-photon-excited and two-photon-excited fluorescence imaging. In addition, bis(TPA)-containing **2c**-based devices exhibit dual-emission with good performance with an EQE_{max} of 3.5% and a maximum brightness of 8338 cd/m^2. The singlet exciton yield of the device is 92% breaking through the theoretical limit of 25% in conventional fluorescent OLEDs. This is one of the highest exciton utilization value recorded for the ESIPT molecules with a dual emission system. This work unlocks an opportunity to rapidly synthesize the high-performance and multifunctional fluorescent materials, which can be used in mechanochromic luminescence, imaging, and high-performance OLED fabrication.

Declaration of competing interests

The authors declare that they have no known competing financial interests or personal relationships that could have appeared to influence the work reported in this paper.

Acknowledgments

We thank Jiangsu Key Laboratory of Advanced Catalytic Materials and Technology (No. BM2012110), the fundamental research funds for the central universities (No. 2023CDJYGRH-YB17), the Venture & Innovation Support Program for Chongqing Overseas Returnees (No. cx2022061), the Natural Science Foundation of Chongqing (No. CSTB2022NSCQ-MSX1123), the Chongqing Talents: Exceptional Young Talents Project (No. cstc2021ycjh-bgzxm0067), Changzhou University, Advanced Catalysis and Green Manufacturing Collaborative Innovation Center (No. ACGM2022–10–10), and National Natural Science Foundation of China (Nos. 21702019, 62174160) for financial support. We also thank Prof. Jingsong You for the helpful discussions, and Mrs. Qin Deng (Chongqing University analysis and testing center) for fluorescence imaging.

Supplementary materials

Supplementary material associated with this article can be found, in the online version, at doi:10.1016/j.cclet.2024.109554.

References

[1] B. Li, A.I.M. Ali, H. Ge, Chem 6 (2020) 2591–2657.
[2] K.M. Wang, J.X. Zhang, R.K. Hu, et al., ACS Catal. 12 (2022) 2796–2820.
[3] C.L. Chen, Y.T. Chen, A.P. Demchenko, P.T. Chou, Nat. Rev. Chem. 2 (2018) 131–143.
[4] C.C. Hsieh, C.M. Jiang, P.T. Chou, Acc. Chem. Res. 43 (2010) 1364–1374.
[5] J.E. Kwon, S.Y. Park, Adv. Mater. 23 (2011) 3615–3642.
[6] A.P. Demchenko, K.C. Tang, P.T. Chou, Chem. Soc. Rev. 42 (2013) 1379–1408.
[7] V.S. Padalkar, S. Seki, Chem. Soc. Rev. 45 (2016) 169–202.
[8] J. Wu, Y.Y. Cheng, J.B. Lan, et al., J. Am. Chem. Soc. 138 (2016) 12803–12812.
[9] G.C. Li, F.J. Song, D. Wu, et al., Adv. Funct. Mater. 24 (2014) 747–753.
[10] Y. Sagara, S. Yamane, M. Mitani, C. Weder, T. Kato, Adv. Mater. 28 (2016) 1073–1095.
[11] B. Li, H. Ge, Sci. Adv. 5 (2019) eaaw2774.
[12] B. Li, K. Seth, B. Niu, et al., Angew. Chem. Int. Ed. 57 (2018) 3401–3405.
[13] B. Li, B. Lawrence, G. Li, H. Ge, Angew. Chem. Int. Ed. 59 (2020) 3078–3082.
[14] D. Zhao, G. Li, D. Wu, et al., Angew. Chem. Int. Ed. 52 (2013) 13676–13680.
[15] Q. Huang, Q. Guo, J.B. Lan, et al., Mater. Horiz. 8 (2021) 1499–1508.
[16] D.X. Cao, Z.Q. Liu, P. Verwilst, et al., Chem. Rev. 119 (2019) 10403–10519.
[17] A.B. Chinen, C.M. Guan, J.R. Ferrer, et al., Chem. Rev. 115 (2015) 10530–10574.
[18] T.B. Ren, Z.Y. Wang, Z. Xiang, et al., Angew. Chem. Int. Ed. 60 (2021) 800–805.
[19] Y. Cheng, G. Li, Y. Liu, et al., J. Am. Chem. Soc. 138 (2016) 4730–4738.
[20] J. Shi, P.W. Kantoff, R. Wooster, O.C. Farokhzad, Nat. Rev. Cancer 17 (2017) 20–37.
[21] Y. Xu, P. Xu, D. Hu, Y. Ma, Chem. Soc. Rev. 50 (2021) 1030–1069.
[22] Z. Chen, H. Qin, Y. Yin, et al., Chem. Eur. J. 29 (2023) e202203797.
[23] X. Wang, Z. Chen, J. Yin, S.H. Liu, Chin. Chem. Lett. 33 (2022) 2522–2526.
[24] Y. Yin, Z. Chen, R. Li, et al., Inorg. Chem. 60 (2021) 9387–9393.
[25] M. Durko-Maciag, G. Ulrich, D. Jacquemin, J. Mysliwiec, J. Massue, Phys. Chem. Chem. Phys. 25 (2023) 15085–15098.
[26] H. Gu, W. Wang, W. Wu, et al., Chem. Commun. 59 (2023) 2056–2071.
[27] T. Iijima, A. Momotake, Y. Shinohara, et al., J. Phys. Chem. A 114 (2010) 1603–1609.
[28] J. Seo, S. Kim, S.Y. Park, J. Am. Chem. Soc. 126 (2004) 11154–11155.
[29] L. Yao, S. Zhang, R. Wang, et al., Angew. Chem. Int. Ed. 53 (2014) 2119–2123.
[30] C.W. Lin, P.B. Han, S. Xiao, et al., Adv. Funct. Mater. 31 (2021) 2106912.
[31] A. Obolda, M. Zhang, F. Li, Chin. Chem. Lett. 27 (2016) 1345–1349.
[32] Y. Luo, Z. Lu, Y. Huang, Chin. Chem. Lett. 27 (2016) 1223–1230.
[33] Y. Shen, X. Tang, Y. Xu, et al., Chin. Chem. Lett. 30 (2019) 1947–1950.
[34] X. Dong, S. Shen, Y. Qin, et al., Chin. Chem. Lett. 34 (2023) 108311.
[35] K. Wang, R. Hu, J. Wang, et al., ACS Mater. Lett. 4 (2022) 2337–2344.
[36] B. Li, J. Lan, D. Wu, J. You, Angew. Chem. Int. Ed. 54 (2015) 14008–14012.
[37] B. Li, L. Zhou, H. Cheng, et al., Chem. Sci. 9 (2018) 1213–1220.
[38] S. Park, J.E. Kwon, S.H. Kim, et al., J. Am. Chem. Soc. 131 (2009) 14043–14049.
[39] K.C. Tang, M.J. Chang, T.Y. Lin, et al., J. Am. Chem. Soc. 133 (2011) 17738–17745.
[40] W. Li, Y. Pan, R. Xiao, et al., Adv. Funct. Mater. 24 (2014) 1609–1614.
[41] S. Zhang, L. Yao, Q. Peng, et al., Adv. Funct. Mater. 25 (2015) 1755–1762.
[42] T. Liu, L. Zhu, C. Zhong, et al., Adv. Funct. Mater. 27 (2017) 1606384.
[43] W. Li, D. Liu, F. Shen, et al., Adv. Funct. Mater. 22 (2012) 2797–2803.